

†Department of Biology, California State University, Fresno, California 93740, USA
 ‡Università di Pisa, Dipartimento di Etologia, Ecologia ed Evoluzione, 56126 Pisa, Italy
 §Merkel and Associates, San Diego, California 92123, USA
 ||Royal Botanic Gardens, Sydney, New South Wales 2000, Australia
 ¶Université de Nice-Sophia Antipolis, Laboratoire Environnement Marin Littoral, 06108 Nice, France

Imaging
Phase radiography with neutrons

The interaction of neutrons with matter enables neutron radiography¹ to complement X-ray radiography in analysing materials. Here we describe a simple quantitative method that provides a new contrast mechanism for neutron radiography and allows samples to be imaged at low radiation doses. Large phase shifts can be measured accurately from detailed structures not amenable to conventional techniques.

The complexity of interferometry has limited studies on neutron phase imaging. Our non-interferometric phase-measurement technique is appropriate for non-uniform radiation and returns a unique, non-wrapped, smooth, continuous quantitative phase map; it implements a theoretical study² and has been used for other types of radiation, including visible light³, electrons⁴, soft⁵ and hard⁶ X-rays.

We base our analysis on the paraxial transport of intensity equation^{7,8}

$$\frac{2\pi}{\lambda} \frac{\partial I(\mathbf{r}_\perp)}{\partial z} = -\nabla_\perp \times [I(\mathbf{r}_\perp) \nabla_\perp \phi(\mathbf{r}_\perp)] \quad (1)$$

where the wave is described by $\sqrt{I(\mathbf{r}_\perp)} \exp(i\phi(\mathbf{r}_\perp))$, with intensity $I(\mathbf{r}_\perp)$ and phase $\phi(\mathbf{r}_\perp)$; ∇_\perp and \mathbf{r}_\perp are respectively the gradient operator and position vector in the plane perpendicular to the longitudinal optic axis z , λ is the wavelength, and $\partial I(\mathbf{r}_\perp)/\partial z$ is the longitudinal intensity derivative.

We used the beam port of the Neutron Interferometry facility at NIST, operating at a selectable monochromatic wavelength of 4.43 Å. The divergence of the neutron beam was limited by a mask to around 6 milliradians and neutrons illuminated a sample at about 1.8 m from the beam-guide exit. The two-dimensional detector⁹ was 30% efficient and combined an in-beam ⁶Li-ZnS scintillator, light intensifier and mirror. The mirror reflected the light out of the neutron beam and into an optical charge-coupled device camera. Electronic centroiding of images optimized the spatial resolution to 60 μm.

The intensity over a surface is consistent

1. Kaiser, J. *Science* **289**, 222–223 (2000).
2. Dalton, R. *Nature* **406**, 447 (2000).
3. Meinesz, A. & Boudouresque, C. F. *C. R. Acad. Sci. Paris Life Sci.* **319**, 603–613 (1996).
4. Meinesz, A. & Hesse, B. *Oceanol. Acta* **14**, 415–426 (1991).
5. Jousson, O., Pawlowski, J., Zaninetti, L., Meinesz, A. & Boudouresque, C. F. *Mar. Ecol. Prog. Ser.* **172**, 275–280 (1998).
6. Meinesz, A. *et al. Bot. Mar.* **38**, 499–508 (1995).
7. Komatsu, T., Meinesz, A. & Buckles, D. *Mar. Ecol. Prog. Ser.* **146**, 145–153 (1997).
8. Olsen, J. L., Valero, M., Meusnier, I., Boele-Bos, S. & Stam, W. T. *J. Phycol.* **34**, 850–856 (1998).
9. Pighini, M. & Dini, F. *4th International Workshop on Caulerpa taxifolia* (Lerici, Italy, 1999).

with any phase distribution. Equation (1) indicates, however, that the phase does influence the propagation of the intensity. It is therefore possible to visualize phase in a certain plane by allowing a wave to evolve

away from that plane¹⁰ — an example of this is the familiar heat shimmer over a hot road. This effect was used to visualize the neutron phase shift for a North American yellow-jacket wasp (genus *Vespula*) (Fig. 1). A conventional neutron radiograph (Fig. 1a) is compared with a phase-contrast image obtained 1.8 m downstream from the sample using neutrons emanating from a 0.4-mm-diameter pinhole placed at the exit of the beam guide (Fig. 1b). The pinhole sets the limit to the spatial resolution. The improved sensitivity of the image arises from shifts in the neutron phase introduced by the sample.

To retrieve phase quantitatively using equation (1), we require the intensity $I(\mathbf{r}_\perp)$ and intensity derivative $\partial I(\mathbf{r}_\perp)/\partial z$ in the plane of interest. To obtain this, images were

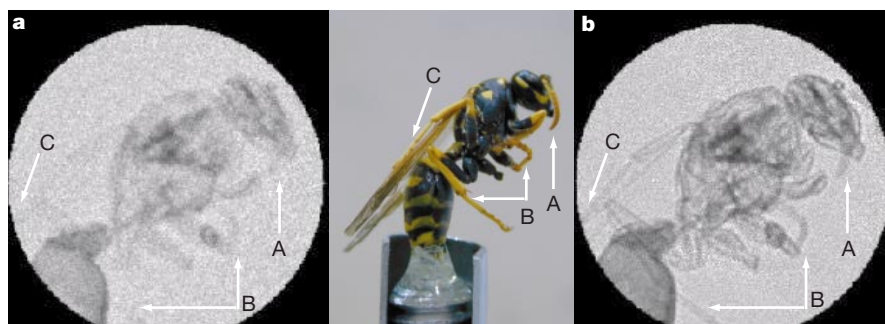


Figure 1 Neutron phase-contrast imaging of a yellow-jacket wasp. **a**, Conventional neutron radiograph. **b**, Phase-contrast image showing greater clarity of finer features such as the antenna (A), legs (B) and projection through the leg and wing (C).

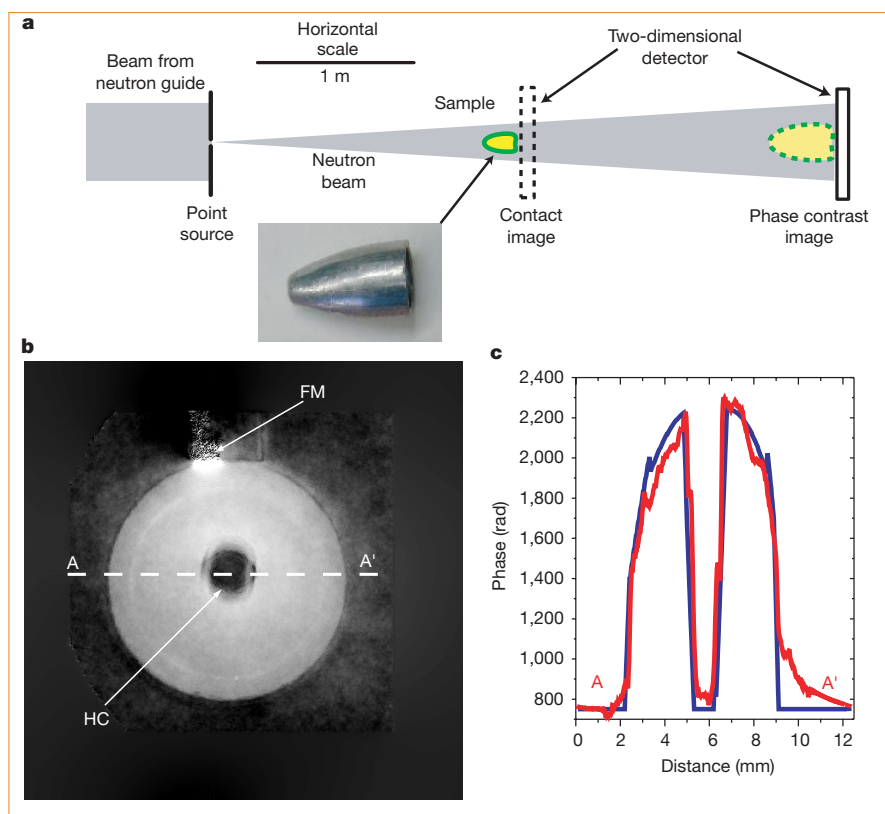


Figure 2 Quantitative neutron phase imaging. **a**, Experimental scheme, with the lead sinker sample shown in the inset. **b**, Quantitative phase map of the Pb sinker showing the hollow core (HC) and fiducial mark artefact (FM). **c**, Quantitative phase profile AA' through the sinker (red) and calculated profile (blue) based on the known shape, scattering length and orientation of the sinker.

taken in two planes: the first was a contact image and the second was a phase-contrast image with the detector 1.8 m from the object (Fig. 2a). Using the contact image and the phase-contrast image, we approximate the intensity by their average, and the intensity derivative by their difference divided by their separation. We used this approach to image a sinker made of lead aligned longitudinally with the beam (Fig. 2a, inset). The measured phase from equation (1) is shown in Fig. 2b. The phase deformity is an artefact of a gadolinium fiducial mark; the hollow core can be clearly seen in the phase image.

The phase image obtained is, to a good approximation, described by a convolution of the perfect image with the intensity distribution of the effective source. In our analysis, we used a very conservative estimate of the effective width of the neutron source to modify the phase-recovery algorithm. A profile of the recovered phase is plotted in Fig. 2c, together with the predicted phase profile determined from the sample geometry, scattering length and orientation, and gives good quantitative agreement between the two. Note that the 1,400-rad phase excursion of the sample occurs in a few hundred micrometres (less than ten pixels). An interferometric experiment would require submicrometre resolution to measure such a rapid phase excursion accurately.

This simple and general technique provides independent quantitative phase and absorption images of the sample. These images constitute two-dimensional projections of the real and imaginary parts of the neutron refractive-index distribution through a three-dimensional object. A number of these projections could be used to generate a quantitative tomographic reconstruction.

B. E. Allman*, **P. J. McMahon***,
K. A. Nugent*, **D. Paganin***,
D. L. Jacobson†, **M. Arif†**, **S. A. Werner‡**

*School of Physics, University of Melbourne,
Victoria 3010, Australia

e-mail: k.nugent@physics.unimelb.edu.au

†Physics Laboratory, National Institute of Standards
and Technology (NIST), Gaithersburg,
Maryland 20899, USA

‡Department of Physics and Astronomy,
University of Missouri-Columbia, Columbia,
Missouri 65211, USA

- Schlenker, M. & Baruchel, J. *Physica B* **137**, 309–319 (1986).
- Paganin, D. & Nugent, K. A. *Phys. Rev. Lett.* **80**, 2586–2589 (1998).
- Barty, A., Nugent, K. A., Paganin, D. & Roberts, A. *Opt. Lett.* **23**, 817–819 (1998).
- Bajt, S. *et al. Ultramicroscopy* **83**, 67–73 (2000).
- Allman, B. E. *et al. J. Opt. Soc. Am. A* **17**, 1732–1743 (2000).
- Nugent, K. A., Gureyev, T. E., Cookson, D., Paganin, D. & Barnea, Z. *Phys. Rev. Lett.* **77**, 2961–2964 (1996).
- Teague, M. R. *J. Opt. Soc. Am.* **73**, 1434–1441 (1983).
- Gureyev, T. E., Roberts, A. & Nugent, K. A. *J. Opt. Soc. Am. A* **12**, 1942–1946 (1995).
- Dietze, M., Felber, J., Raum, K. & Rausch, C. *Nucl. Inst. Meth. A* **377**, 320–324 (1996).
- Zernike, F. *Physica* **9**, 686–693 (1942).

Scaling

Rivers, blood and transportation networks

The search for a theory to explain why the metabolic rate of mammals is proportional to the 3/4-power of body mass (Kleiber's law) has recently focused on the nutrient distribution network formed by arteries and capillaries. Banavar *et al.*¹ argue that the law follows from the intrinsic properties of an outward-directed network. But careful analysis of their arguments reveals two implicit assumptions that may not be generally correct. Unless these assumptions are valid for mammalian circulation, these arguments cannot satisfactorily explain Kleiber's empirical relationship.

In the analysis by Banavar *et al.*¹, there is a site for nutrient uptake at each network-branching point, and the distance L_x along a path from the origin O (the heart) to a site X is defined as the number of uptake sites on the path. The rate of uptake of nutrients at a site is a constant F_x (assumed to be species- and size-invariant). A network segment that goes from a site X to an adjacent site Y is termed the link XY , and the rate at which nutrient enters the link is termed the current and is denoted by I_{XY} . In an outward-directed network (ODN), the direction of flow is away from O on each link.

The authors' fundamental result is that, in an ODN, $C = B \langle L_x \rangle$, where C , the total current in the network, is the sum of currents on all links, B is the metabolic rate (sum of uptake rates), and $\langle L_x \rangle$ is the average distance to sites. The number of uptake sites is expressed as L^3 , and the metabolic rate B is therefore $F_x L^3$. Banavar *et al.* prove that, if $\langle L_x \rangle$ is proportional to L , if C is proportional to blood volume V_b , and if V_b is proportional to body size M , then B is proportional to $M^{3/4}$, which is Kleiber's law.

Although the assumption that $V_b \propto M$ is a reasonable approximation, the assumption that $C \propto V_b$ is not, in general, true. Consider a network formed by $(l-1)(m-1)(n-1)$ unit cubes stacked to form a rectangle $(l-1)$ units deep by $(m-1)$ units wide by $(n-1)$ units high. Each vertex of a cube is an uptake site and each edge is a network link with constant cross-sectional area. Current is supplied to the bottom rear left corner of the network and flows forward, rightward and upward. It follows from induction on n that the sum of currents in all vertical links is $lmn(n+1)F_x/2$. Adding the corresponding expressions for currents flowing rightward and forward gives $lmnF_x(l+m+n+3)/2$, the total current C . The blood in the network is proportional to the number of links, $3lmn - lm - ln - mn$. Thus, in this model, in which the density of uptake sites is invariant, C is nearly proportional to volume multiplied by average linear dimension, metabo-

lism is proportional to volume, and V_b is approximately proportional to volume.

The relation between V_b and C depends on parameters that do not appear in Banavar *et al.*'s report¹. The volume of blood in link XY is equal to the cross-sectional area of the link (A_{XY}) multiplied by the length of the link (s_{XY}), whereas current I_{XY} is A_{XY} multiplied by flow velocity (f_{XY}). The volume of blood in a link is therefore $I_{XY}s_{XY}/f_{XY}$. The assumption that the sum of currents equals (or scales as) total blood volume implies that the average value of s_{XY} increases as size increases. In arteries, the flow velocity may increase as size increases, but flow rates in capillaries are severely constrained by their relatively constant cross-sectional area and pressure. If most uptake sites are located in capillary networks, the currents in capillaries comprise most of the sum C , but the blood in these vessels may comprise a minority of blood volume.

The assumption that $\langle L_x \rangle \propto L$ is also not true in general in an ODN. For example, consider a network that starts with a single link and bifurcates at each branch point until a terminal uptake site is reached at distance k . The number of uptake sites, L^3 , is $2^k - 1$ and $\langle L_x \rangle$ is $[(k-1)2^k - 1]/(2^k - 1)$. Therefore $\langle L_x \rangle$ is approximately proportional to the logarithm of L in this type of ODN.

Page R. Painter

Office of Environmental Health Hazard Assessment,
California Environmental Protection Agency,
301 Capitol Mall, Sacramento,
California 95814-4327, USA
e-mail: ppainter@oehha.ca.gov

The long-standing problem of explaining metabolic scaling² in animals, whereby whole-animal metabolic rate B is observed to increase as a function of body mass M approximately as $M^{3/4}$, has been recently revisited by Banavar *et al.*¹ (see also ref. 3, in which allometric scaling rules are derived from fractal geometry). These authors¹ derive and generalize to non-biological systems, including river networks, a three-quarter-power 'allometric' scaling rule, which arises, in their treatment, from an assumption of the efficiency of the resource distribution network. Here I present a simple derivation of 3/4-power scaling based on the geometric requirements of inventorying resources before metabolization, which does not support the notion of allometric scaling suggested by Banavar *et al.*¹ for rivers, at least not when applied to the problem of fluvial sediment transport. Although some distributary systems 'metabolize' according to the 3/4-power rule, this rule is not golden — each system needs to be investigated on its own merits.

As a resource distribution and processing (metabolizing) system increases in size, there is a geometric necessity for an incompressible and conserved resource for